

Dirac zeros in an orbital selective Mott phase: Green's function Berry curvature and flux quantization

Lei Chen¹, Haoyu Hu^{2,1}, Maia G. Vergniory^{2,3}, Jennifer Cano^{4,5}, and Qimiao Si¹

¹*Department of Physics and Astronomy, Rice Center for Quantum Materials, Rice University, Houston, Texas 77005, USA*

²*Donostia International Physics Center, P. Manuel de Lardizabal 4, 20018 Donostia-San Sebastian, Spain*

³*Max Planck Institute for Chemical Physics of Solids, Noethnitzer Str. 40, 01187 Dresden, Germany*

⁴*Department of Physics and Astronomy, Stony Brook University, Stony Brook, NY 11794, USA and*

⁵*Center for Computational Quantum Physics, Flatiron Institute, New York, NY 10010, USA*

How electronic topology develops in strongly correlated systems represents a fundamental challenge in the field of quantum materials. Recent studies have advanced the characterization and diagnosis of topology in Mott insulators whose underlying electronic structure is topologically nontrivial, through “Green’s function zeros”. However, their counterparts in metallic systems have yet to be explored. Here, we address this problem in an orbital-selective Mott phase (OSMP), which is of extensive interest to a variety of strongly correlated systems with a short-range Coulomb repulsion. We demonstrate symmetry protected crossing of the zeros in an OSMP. Utilizing the concept of Green’s function Berry curvature, we show that the zero crossing has a quantized Berry flux. The resulting notion of Dirac zeros provides a window into the largely hidden landscape of topological zeros in strongly correlated metallic systems and, moreover, opens up a means to diagnose strongly correlated topology in new materials classes.

Introduction. Quantum fluctuations as promoted by strong correlations drive novel electronic phases of matter [1, 2], and this also applies when the underlying electronic structure is topologically nontrivial [3–10]. One important question is how to diagnose electronic topology in the strongly correlated settings. In band theory of non-interacting crystalline systems, lattice symmetries constrain the one-electron eigenstates—the Bloch states—and serve as indicators for topology [11–16]; they uniquely determine the representations [14] of the Bloch states and justify the robustness of band degeneracies in the energy dispersion [17]. In interacting systems, a fundamental quantity is the single-particle Green’s function [18], which describes the frequency and wavevector-resolved propagation of an electron in the many-particle environment. The eigenvectors of the Green’s function form a representation of the space group [19]. In addition, these eigenvectors allow for the introduction of a Green’s function Berry curvature [20].

Mott insulators develop when the Coulomb repulsion is strong (and the band filling is commensurate). They have been known to feature Green’s function zeros [21–23], contours in frequency-momentum space at which the Green’s function vanishes. The roles of these zeros in the topology of Mott insulators have recently gained considerable interest [24, 25] in the presence of topological non-interacting bands [26]. In particular, it was shown that symmetry constraints based on Green’s function eigenvectors also act on the zeros [24]. Moreover, the notion of Green’s function Berry flux quantization has been illustrated in a Mott insulator derived from long-ranged interactions [20]. The quantized flux of the zeros serves as a means to search for topological Mott insulators.

In this work, we address whether and how Green’s function zeros can play a role in the topology of corre-

lated metallic systems. To this end, we study an orbital-selective Mott phase, arising in correlated multi-orbital systems when a subset of the orbitals are (on the verge of being) localized. OSMP and its proximate regimes are increasingly being recognized as important to a variety of strongly correlated materials platforms [2, 27–39]. Furthermore, we consider a local Coulomb repulsion. We show that symmetry protected zero crossings occur and demonstrate the notion of Dirac zeros in terms of a quantization of the Green’s function Berry flux. Given that the orbital-selective Mott physics is prevalent across the strongly correlated metallic systems, our work opens up an important new avenue to realize strongly correlated topological matter.

Model and Methods. We consider a four-orbital interacting Hamiltonian defined on a cubic lattice, taking the form of $\mathcal{H} = \mathcal{H}_0 + \mathcal{H}_{int}$.

The noninteracting part preserves a U(1)-spin rotational symmetry along the z -axis; in accordance, $\mathcal{H}_0^\uparrow = [\mathcal{H}_0^\downarrow]^\dagger$. The kinetic Hamiltonian for the spin- \uparrow electrons is given by $\mathcal{H}_0^\uparrow = \sum_{\mathbf{k}} \Psi_{\mathbf{k}\uparrow}^\dagger H_0^\uparrow(\mathbf{k}) \Psi_{\mathbf{k}\uparrow}$, where $\Psi_{\mathbf{k}\uparrow} = [\psi_{Ah\uparrow}, \psi_{Bh\uparrow}, \psi_{Al\uparrow}, \psi_{Bl\uparrow}]^T$, with subscripts $\tau = A/B$ and $o = h/l$ introduced to distinguish the sublattices and heavy/light orbitals, respectively.

$$H_0^\uparrow(\mathbf{k}) = \begin{pmatrix} H_{0,hh}^\uparrow(\mathbf{k}) & H_{0,hl}^\uparrow(\mathbf{k}) \\ [H_{0,hl}^\uparrow(\mathbf{k})]^\dagger & H_{0,ll}^\uparrow(\mathbf{k}) \end{pmatrix}, \quad (1)$$

in which $H_{0,hh/ll}^\uparrow(\mathbf{k}) = 2t_h/t_l(\cos k_x + \cos k_y + \cos k_z)\tau_z + 2t_{h/l}^{soc}(\sin k_x\tau_x + \sin k_y\tau_y)$ and $H_{0,hl}^\uparrow(\mathbf{k}) = 2t_{hl}(\cos k_x + \cos k_y + \cos k_z)$. $\tau_{x/y/z}$ are the Pauli matrices acting on the sublattice space. Furthermore, t_h (t_l) and t_h^{soc} (t_l^{soc}) denote the nearest neighbor direct hopping and spin-orbit coupling between the heavy (light) orbitals, re-

spectively, while t_{hl} represents the nearest neighbor hopping between the heavy and light orbitals. We consider $|t_h|$ to be considerably smaller than $|t_l|$, such that for the same interaction strength, the heavy orbitals are much more correlated than the light orbitals. Without a loss of generality, we adopt the following parameters: $t_h = 1$, $t_h^{soc} = 0.6$, $t_l = 4$, $t_l^{soc} = 2.4$ and $t_{hl} = 1.5$.

We will consider the effect of an onsite Coulomb repulsion. Our focus will be on a range of interactions that are small compared to the light bandwidth and, accordingly, have a relatively weak effect on the light band. Thus, for simplicity, we will study only the effect of an intraorbital Hubbard interaction that acts on the heavy orbitals:

$$\mathcal{H}_{int} = \sum_{\tau} \frac{U}{2} (n_{\tau h \uparrow} + n_{\tau h \downarrow} - 1)^2, \quad (2)$$

where the index τ enumerates the two sublattices of the heavy orbitals. The model contains a C_{4z} rotational symmetry, which protects the gapless Dirac points in the weak coupling region.

Dispersive zeros may arise only if the electron self-energy is \mathbf{k} -dependent. To capture such effects, we develop a cluster version of the U(1)-slave-spin (SS) method [40]. In the U(1)-SS approach, an electronic operator is expressed as $\psi_{i\tau\sigma}^{\dagger} = S_{i\tau\sigma}^{+} f_{i\tau\sigma}^{\dagger}$, where the SS operator S^{+} is introduced to carry the charge degree of freedom and the auxiliary fermion f^{\dagger} the spin degree of freedom in the form of a ‘‘spinon’’ operator. The enlarged Hilbert space spanned by the SS and auxiliary fermion is limited to the physical ones when we impose the constraint $S_{i\tau\sigma}^z + 1/2 = f_{i\tau\sigma}^{\dagger} f_{i\tau\sigma}$. We treat the Hamiltonian in the SS representation at the saddle-point level, which leads to two decoupled effective Hamiltonians, each containing only the SS or auxiliary fermions, respectively [See the supplementary materials (SM)]. Furthermore, we exactly diagonalize the SS Hamiltonian which is constrained on a finite cluster that is embedded in an effective medium; here, we consider a cluster size of two unit cells.

The Mott transition of an orbital is signaled by the vanishing of its quasiparticle weight, which is determined from $Z_{i\tau\sigma} = |\langle S_{i\tau\sigma}^{+} \rangle|^2$. The spatial fluctuations are captured by the bond operators $\chi_{i\tau\sigma, j\tau'\sigma'}^f = \langle S_{i\tau\sigma}^{+} S_{j\tau'\sigma'}^{-} \rangle$. Further details of the method and its context are given in the SM.

Orbital selective Mott phase. In the noninteracting limit, the Hamiltonian describes two species of semimetals, each associated with one kind of orbital and each having four gapless (Dirac) points sitting at the momenta $(\pi, 0, \pm\frac{\pi}{2})$ and $(0, \pi, \pm\frac{\pi}{2})$. The system contains both the time-reversal (\mathcal{T}) and inversion (\mathcal{Z}) symmetries. The discrete rotation C_{4z} symmetry protects the Dirac crossings along the high symmetry lines paralleled to the z -axis. The noninteracting band structure along the high symmetry line $X - R$ is displayed in Fig. 1(b), showing a symmetry protected Dirac node.

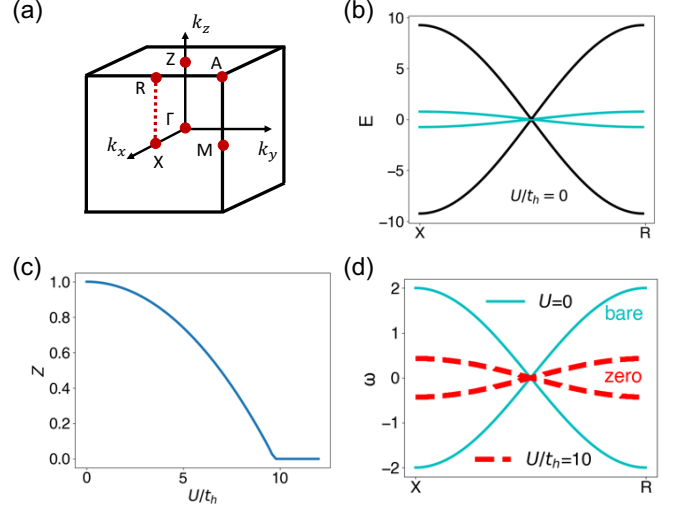


FIG. 1. (a) Brillouin zone of a cubic lattice, with high symmetry points marked. (b) The non-interacting band structure of the narrow (cyan) and wide (black) bands along a high symmetry line ($X - R$), showing a Dirac node protected by symmetry. (c) Quasiparticle weight of the heavy electrons as a function of the onsite interaction U . (d) Red dashed lines: Green’s function zeros in the OSMP phase, for $U/t_h = 10$, dispersing along $X - R$. Cyan solid lines: Dispersion of the bare narrower-band electrons, at $U = 0$.

We are now in position to discuss the correlation effect. As depicted in Fig. 1(c), the quasiparticle weight of the heavy orbitals monotonically decreases as we increase the strength of the intra-orbital on-site Hubbard interaction. It eventually diminishes to zero at a critical value $U_c/t_h = 9.5$. Notice that, the effective interorbital hybridization between the heavy and light electrons equals to $\sqrt{Z_h} t_{hl}$, which also vanishes in the OSMP. In other words, the heavy electrons are decoupled from the light ones in the OSMP, leading to the notion of correlation-driven dehybridization, which is analogous to the Kondo-destroyed fixed point of heavy fermion systems [28–30]. Such a dehybridization fixed point is realized from the competition between the hybridization and spatial correlations, which protects the stability of the OSMP [41, 42].

Dirac nodes of Green’s function zeros. We now turn to the single particle Green’s function. In the SS approach, it is represented by the SS and auxiliary fermions as $G_{\sigma}^{\tau\sigma\tau'o'}(i - j, \tau) = -\langle T_{\tau} S_{i\tau\sigma}^{-}(\tau) S_{j\tau'o'\sigma}^{+}(0) f_{i\tau\sigma}(\tau) f_{j\tau'o'\sigma}^{\dagger}(0) \rangle$. At the saddle-point level, the Green’s function is decomposed into coherent and incoherent parts as follows:

$$G^{\tau\sigma\tau'o'}(\mathbf{k}, i\omega_n) = \sqrt{Z_{\tau\sigma} Z_{\tau'o'}} G_f^{\tau\sigma\tau'o'}(\mathbf{k}, i\omega_n) + G_{incoh}^{\tau\sigma\tau'o'}(\mathbf{k}, i\omega_n). \quad (3)$$

In the coherent part, $G_f^{\tau\sigma\tau'o'}$ represents the Green’s function of the auxiliary fermion. In our case, the quasipar-

title weights ($Z_{\tau l}$) for the light orbitals are equal to 1 across the whole phase diagram. In the OSMP phase, the heavy electrons completely lose their coherence and, thus, the coherent part of the Green's function is entirely comprised of the light orbitals. On the other hand, the incoherent part of the Green's function is uniquely contributed by the heavy orbitals. The momentum-resolved incoherent Green's function is obtained by a Fourier transform of the real space counterpart. This leads to

$$G_{incoh}^{\tau\sigma\tau'o'}(\mathbf{k}, i\omega_n) = G_{incoh}^{\tau\sigma\tau'o'}(\mathbf{0}, i\omega_n) + \sum_{\mathbf{R} \neq \mathbf{0}} e^{i\mathbf{k} \cdot \mathbf{R}} G_{incoh}^{\tau\sigma\tau'o'}(\mathbf{R}, i\omega_n), \quad (4)$$

where \mathbf{R} enumerates through the separations between the unit cells. The specific expressions of $G_{incoh}^{\tau\sigma\tau'o'}(\mathbf{0}, i\omega_n)$ and $G_{incoh}^{\tau\sigma\tau'o'}(\mathbf{R}, i\omega_n)$ are shown in the SM.

We focus on the OSMP, which is illustrated with the choice of the interaction strength $U/t_h = 10$. We calculate the determinant of the retarded Green's function $|\det G(\mathbf{k}, \omega + i0^+)|$ for the heavy orbitals in order to look for the zeros of the interacting single-particle Green's function.

To further elaborate on the electronic properties in the OSMP, we show the spectrum function for the heavy orbitals in Fig. 2(a), which is calculated from $\rho^h(\mathbf{k}, \omega) = -\frac{1}{\pi} \sum_{\tau\sigma} G_{\sigma}^{\tau h \tau h}(\mathbf{k}, \omega + i0^+)$. The lower and upper Hubbard bands are separated by a Mott gap as marked by the arrow shown in Fig. 2(a). We then turn to discussing the frequency resolved determinant of the Green's function. Its frequency dependence at $\mathbf{k} = (\pi, 0, 0)$ and $\mathbf{k} = (\pi, 0, \frac{\pi}{2})$ is respectively displayed in Figs. 2(b,c) on a logarithmic scale. The lower and upper Hubbard bands correspond to the broad shoulder-like peaks at high frequencies. Whereas the Green's function zeros, marked by the black arrows, reside within the Mott gap. Different from the case of momentum X , which is shown in Fig. 2(b), only one dip is observed at momentum $\mathbf{k} = (\pi, 0, \pi/2)$ [Fig. 2(c)], showing that the Green's function zeros are merged at this momentum.

The collection of zeros at the different wavevectors is depicted in Fig. 1(d). The red dashed lines show the dispersive zeros along the high symmetry line $X - R$. Furthermore, two branches of Green's function zeros merge exactly at momentum for the Dirac node of the bare heavy electrons in the noninteracting limit, which are denoted by the cyan solid lines in Fig. 1(d). (Here, "bare" means both at $U = 0$ and without a hybridization between the heavy and light electrons.) This result demonstrates the presence and robustness of the "gapless" node coming from the Green's function zeros in the strongly correlated limit, and motivates us to use the eigenvectors of the Green's function zeros (instead of Green's function poles) to diagnose the topology in such strongly correlated systems.

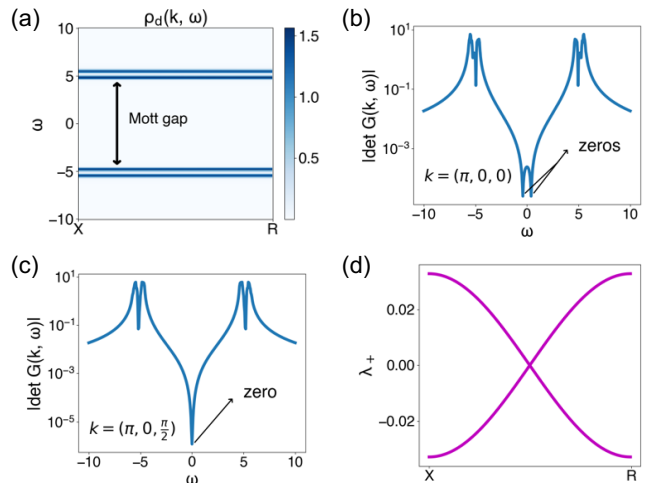


FIG. 2. (a) The energy distribution of the total spectral function along $X - R$, at $U/t_h = 10$. The Mott gap is marked. (b) and (c), The variance of $|\det G(\mathbf{k}, \omega)|$ for the heavy orbitals versus ω , demonstrating the Green's function zeros, at $\mathbf{k} = (\pi, 0, 0)$ and $\mathbf{k} = (\pi, 0, \pi/2)$, respectively, (d) Eigenvalues of $G_+(\mathbf{k}, \omega)$ at fixed frequency $\omega = 0$, along the high symmetry line $X - R$.

Quantization of Green's function Berry flux. In the noninteracting limit, the winding of the Bloch functions in the momentum space is used to calculate the Berry flux quantization. The question is how to define an appropriate Berry phase for the strongly correlated case. Here, we use a frequency-dependent Berry curvature from the Green's function eigenvectors, which has recently been introduced [20].

We define a Hermitian combination:

$$G_+(\mathbf{k}, \omega) = G^R(\mathbf{k}, \omega) + G^A(\mathbf{k}, \omega), \quad (5)$$

where $G^{R,A}$ are the retarded and advanced Green's functions. We focus on this combination (as opposed to, say, G_+^{-1}) because it is regular across the zeros in the frequency-momentum space. The α -th eigenvalues and eigenvectors of the new Green's function are obtained by the eigenvalue equation,

$$G_+(\mathbf{k}, \omega)|\phi_\alpha(\mathbf{k}, \omega)\rangle = \lambda_+^\alpha |\phi_\alpha(\mathbf{k}, \omega)\rangle. \quad (6)$$

Because of the Hermiticity, the eigenvalues λ_+ are always real. The eigenvalues of G_+ at $\omega = 0$ is depicted in Fig. 2(d). Similar to the noninteracting bands and Green's function zeros, along the same high symmetry line, the "band"s show a nodal crossing at the middle point of $X - R$.

Furthermore, from the "energy" (eigenvalues λ_+) of the "bands", we are able to define the Berry curvature associated with the eigenvectors at momentum \mathbf{k} and fre-

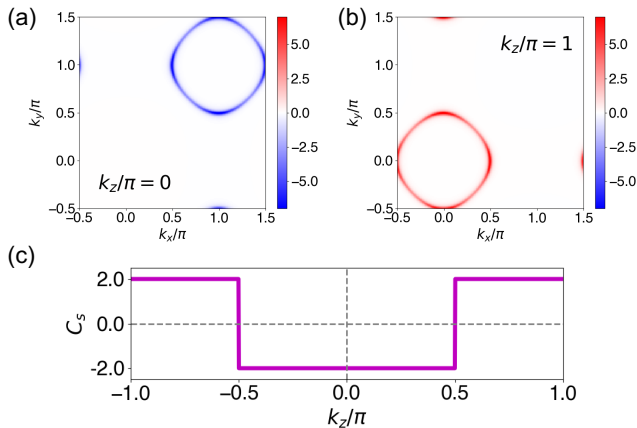


FIG. 3. (a) and (b), The Green's function Berry curvature, $B_z^\dagger(\mathbf{k}, \omega)$, for frequency $\omega = 0$, in the $k_z = 0$ and $k_z = \pi$ planes, respectively. (c) The spin Chern number obtained from the Green's function Berry curvature as a variance of k_z at the fixed frequency $\omega = 0$, demonstrating the quantization of the corresponding Berry flux around the Dirac node of zeros.

quency ω . It takes the form of

$$B_m(\mathbf{k}, \omega) = \sum_{\alpha, i, j} \epsilon_{ijm} [\langle \partial_i \phi_\alpha(\mathbf{k}, \omega) | \partial_j \phi_\alpha(\mathbf{k}, \omega) \rangle], \quad (7)$$

where α sums over the “bands” with eigenvalue λ_\pm^α smaller than 0, and ϵ_{ijm} is the Levi-Civita symbol. For a given k_z and ω , a frequency dependent spin Chern number is then calculated by

$$C_s(\omega, k_z) = \frac{i}{2\pi} \sum_{\sigma} (-1)^\sigma \int d\mathbf{k}_\perp B_z^\sigma(\mathbf{k}_\perp, k_z, \omega). \quad (8)$$

with $\mathbf{k}_\perp = (k_x, k_y)$, and $\sigma = 0(1)$ for spin- $\uparrow(\downarrow)$.

We focus on the case $\omega = 0$. The Berry curvatures (spin- \uparrow) at $k_z = 0$ and $k_z = \pi$ planes are displayed in Figs. 3(a,b), which are seen to have different signs. Their distribution in the $k_x - k_y$ plane captures the dispersion of the Green's function “bands”. We find them to be quantized in both planes after integrating the Berry curvature over the whole Brillouin zone plane. We further scan the Chern numbers C_s as a function of k_z , which are shown in Fig. 3(c). There is a sudden jump by a value of 4, when the cutting plane crosses the nodal points at $k_z = \pm\pi/2$. There are two nodes at each of the $k_z = \pi/2$ and $k_z = -\pi/2$ planes (as can be inferred from the SM, Fig. 4). Accordingly, there is a jump of 2 across each crossing.

The quantization of the Berry flux shows an enclosed monopole charge at a touching point of the Green's function bands. Given that the zero crossing has a four-fold degeneracy and a quantized Green's function monopole charge, we will refer to it as a Dirac zero.

Discussion. Several remarks are in order. Firstly,

by using the Green's function Berry flux, we have defined the notion of Dirac zeros. We expect that this can be readily extended to other settings, such as Weyl zeros in correlated systems with broken inversion or time-reversal symmetry. Secondly, our work provides a systematic approach to diagnose the electronic topology in the correlation-driven orbital selective Mott phase. In addition to heavy fermion metals, orbital-selective Mott correlations have been extensively discussed in Fe-based superconductors [32, 33] and are also being recognized in both the moiré structures [34–37] and geometry-induced flat band compounds [38, 39]. Many of these systems contain topological electron bands. As such, the notion of Dirac/Weyl zeros serves as a diagnostic tool to search and obtain new types of strongly correlated topological phases and materials. Finally, it has been increasingly recognized that the Green's function zeros contribute to measurable physical quantities, such as the Luttinger volume [43, 44], Hall effect [44–47] and even quantum oscillations [20, 48] in a consistent way [44]. Consequently, the topological feature defined from Green's function zeros is expected to influence physical properties in a non-trivial manner. This exciting prospect warrants further exploration.

Conclusion. In a multiorbital model with topological bandstructure, we have demonstrated a symmetry protected crossing of Green's function zeros in its orbital-selective Mott phase (OSMP). Through the concept of Green's function Berry curvature, we have found that the four-fold zero crossing carries a quantized monopole charge. Our results show that the Dirac zeros provide a means to search for and realize new type of topological phases in strongly correlated metallic materials. More generally, our work illustrates the power of strong correlations to enable novel topological phases of matter in a broad range of quantum materials.

Note added: After the completion of this work, recent works addressing different models with a focus on edge zeros in strongly interacting topological insulators became available [49, 50].

Acknowledgement. We thank Yuan Fang, Elio König, Gabriela Oprea, Silke Paschen, Chandan Setty, Shouvik Sur, and Fang Xie, for useful discussions. Work at Rice has primarily been supported by the Air Force Office of Scientific Research under Grant No. FA9550-21-1-0356 (model construction, L.C., H.H. and Q.S.), by the National Science Foundation under Grant No. DMR-2220603 and the Robert A. Welch Foundation Grant No. C-1411 (model calculation, L.C. and H.H.), and by the Vannevar Bush Faculty Fellowship ONR-VB N00014-23-1-2870 (conceptualization, Q.S.). The majority of the computational calculations have been performed on the Shared University Grid at Rice funded by NSF under Grant EIA-0216467, a partnership between Rice University, Sun Microsystems, and Sigma Solutions, Inc., the Big-Data Private-Cloud Research Cyber-

infrastructure MRI-award funded by NSF under Grant No. CNS-1338099, and the Extreme Science and Engineering Discovery Environment (XSEDE) by NSF under Grant No. DMR170109. H.H. acknowledges the support of the European Research Council (ERC) under the European Union’s Horizon 2020 research and innovation program (Grant Agreement No. 101020833). M.G.V. acknowledges support to the Spanish Ministerio de Ciencia e Innovación (grant PID2022-142008NB-I00), partial support from European Research Council (ERC) grant agreement no. 101020833 and the European Union NextGenerationEU/PRTR-C17.I1, by the IKUR Strategy under the collaboration agreement between Ikerbasque Foundation and DIPC on behalf of the Department of Education of the Basque Government. as well as by the funding from the Deutsche Forschungsgemeinschaft (DFG, German Research Foundation) through the project FOR 5249 (QUAST). J.C. acknowledges the support of the National Science Foundation under Grant No. DMR-1942447, support from the Alfred P. Sloan Foundation through a Sloan Research Fellowship and the support of the Flatiron Institute, a division of the Simons Foundation. All authors acknowledge the hospitality of the Kavli Institute for Theoretical Physics, UCSB, supported in part by the National Science Foundation under Grant No. NSF PHY-1748958, during the program “A Quantum Universe in a Crystal: Symmetry and Topology across the Correlation Spectrum.” J.C. and Q.S. also acknowledge the hospitality of the Aspen Center for Physics, which is supported by the National Science Foundation under Grant No. PHY-2210452.

-
- [1] B. Keimer and J. E. Moore, *Nat. Phys.* **13**, 1045 (2017).
 [2] S. Paschen and Q. Si, *Nat. Rev. Phys.* **3**, 9 (2021).
 [3] H. L. Stormer, D. C. Tsui, and A. C. Gossard, *Rev. Mod. Phys.* **71**, S298 (1999).
 [4] Y. Xie, A. T. Pierce, J. M. Park, D. E. Parker, E. Khalaf, P. Ledwith, Y. Cao, S. H. Lee, S. Chen, P. R. Forrester, K. Watanabe, T. Taniguchi, A. Vishwanath, P. Jarillo-Herrero, and A. Yacoby, *Nature* **600**, 439 (2021).
 [5] Y. Zeng, Z. Xia, K. Kang, J. Zhu, P. Knüppel, C. Vaswani, K. Watanabe, T. Taniguchi, K. F. Mak, and J. Shan, *Nature* **622**, 69 (2023).
 [6] Z. Lu, T. Han, Y. Yao, A. P. Reddy, J. Yang, J. Seo, K. Watanabe, T. Taniguchi, L. Fu, and L. Ju, arXiv preprint arXiv:2309.17436 (2023).
 [7] H.-H. Lai, S. E. Grefe, S. Paschen, and Q. Si, *Proc. Natl. Acad. Sci. U.S.A.* **115**, 93 (2018).
 [8] S. Dzsaber, L. Prochaska, A. Sidorenko, G. Eguchi, R. Svagera, M. Waas, A. Prokofiev, Q. Si, and S. Paschen, *Phys. Rev. Lett.* **118**, 246601 (2017).
 [9] S. Dzsaber, X. Yan, M. Taupin, G. Eguchi, A. Prokofiev, T. Shiroka, P. Blaha, O. Rubel, S. E. Grefe, H.-H. Lai, Q. Si, and S. Paschen, *Proc. Natl. Acad. Sci. U.S.A.* **118**, e2013386118 (2021).
 [10] L. Chen, C. Setty, H. Hu, M. G. Vergniory, S. E. Grefe, L. Fischer, X. Yan, G. Eguchi, A. Prokofiev, S. Paschen, J. Cano, and Q. Si, *Nat. Phys.* **18**, 134101346 (2022).
 [11] N. P. Armitage, E. J. Mele, and A. Vishwanath, *Rev. Mod. Phys.* **90**, 015001 (2018).
 [12] N. Nagaosa, T. Morimoto, and Y. Tokura, *Nature Reviews Materials* **5**, 621 (2020).
 [13] B. Bradlyn, L. Elcoro, J. Cano, M. G. Vergniory, Z. Wang, C. Felser, M. I. Aroyo, and B. A. Bernevig, *Nature* **547**, 298 (2017).
 [14] J. Cano, B. Bradlyn, Z. Wang, L. Elcoro, M. G. Vergniory, C. Felser, M. I. Aroyo, and B. A. Bernevig, *Phys. Rev. B* **97**, 035139 (2018).
 [15] H. C. Po, A. Vishwanath, and H. Watanabe, *Nature Communications* **8**, 50 (2017).
 [16] H. Watanabe, H. C. Po, M. P. Zaletel, and A. Vishwanath, *Phys. Rev. Lett.* **117**, 096404 (2016).
 [17] J. Cano and B. Bradlyn, *Annu. Rev. Condens. Matter Phys.* **12**, 225 (2021).
 [18] A. A. Abrikosov, L. P. Gorkov, and I. E. Dzyaloshinski, *Methods of quantum field theory in statistical physics* (Courier Corporation, 2012).
 [19] H. Hu, L. Chen, C. Setty, S. E. Grefe, A. Prokofiev, S. Kirchner, S. Paschen, J. Cano, and Q. Si, arXiv preprint arXiv:2110.06182 (2021).
 [20] C. Setty, F. Xie, S. Sur, L. Chen, S. Paschen, M. G. Vergniory, J. Cano, and Q. Si, arXiv preprint arXiv:2311.12031 (2023).
 [21] I. Dzyaloshinskii, *Phys. Rev. B* **68**, 085113 (2003).
 [22] A. M. Essin and V. Gurarie, *Phys. Rev. B* **84**, 125132 (2011).
 [23] Y.-Z. You, Y.-C. He, C. Xu, and A. Vishwanath, *Phys. Rev. X* **8**, 011026 (2018).
 [24] C. Setty, S. Sur, L. Chen, F. Xie, H. Hu, S. Paschen, J. Cano, and Q. Si, arXiv preprint arXiv:2301.13870 (2023).
 [25] N. Wagner, L. Crippa, A. Amaricci, P. Hansmann, M. Klett, E. J. König, T. Schäfer, D. D. Sante, J. Cano, A. J. Millis, A. Georges, and G. Sangiovanni, *Nature Communications* **14**, 7531 (2023).
 [26] T. Morimoto and N. Nagaosa, *Sci. Rep.* **6**, 19853 (2016).
 [27] S. Kirchner, S. Paschen, Q. Chen, S. Wirth, D. Feng, J. D. Thompson, and Q. Si, *Rev. Mod. Phys.* **92**, 011002 (2020).
 [28] Q. Si, S. Rabello, K. Ingersent, and J. Smith, *Nature* **413**, 804 (2001).
 [29] P. Coleman, C. Pépin, Q. Si, and R. Ramazashvili, *J. Phys.: Condens. Matter* **13**, R723 (2001).
 [30] T. Senthil, M. Vojta, and S. Sachdev, *Phys. Rev. B* **69**, 035111 (2004).
 [31] V. Anisimov, I. Nekrasov, D. Kondakov, T. Rice, and M. Sigrist, *The European Physical Journal B-Condensed Matter and Complex Systems* **25**, 191 (2002).
 [32] M. Yi, Y. Zhang, Z.-X. Shen, and D. Lu, *npj Quantum Mater.* **2**, 57 (2017).
 [33] Q. Si and N. E. Hussey, *Phys. Today* **76**, 34 (2023).
 [34] W. Zhao, B. Shen, Z. Tao, Z. Han, K. Kang, K. Watanabe, T. Taniguchi, K. F. Mak, and J. Shan, *Nature* **616**, 61 (2023).
 [35] D. Guerci, J. Wang, J. Zang, J. Cano, J. H. Pixley, and A. Millis, *Sci. Adv.* **9**, eade7701 (2023).
 [36] F. Xie, L. Chen, and Q. Si, arXiv preprint arXiv:2310.20676 (2023).
 [37] W. Zhao, B. Shen, Z. Tao, S. Kim, P. Knüppel, Z. Han, Y. Zhang, K. Watanabe, T. Taniguchi, D. Chowdhury,

- J. Shan, and K. F. Mak, arXiv preprint arXiv:2310.06044 (2023).
- [38] H. Hu and Q. Si, *Sci. Adv.* **9**, eadg0028 (2023).
- [39] J. Huang, C. Setty, L. Deng, J.-Y. You, H. Liu, S. Shao, J. S. Oh, Y. Guo, Y. Zhang, Z. Yue, J.-X. Yin, M. Hashimoto, D. Lu, S. Gorovikov, P. Dai, M. Z. Hasan, Y.-P. Feng, R. J. Birgeneau, Y. Shi, C.-W. Chu, G. Chang, Q. Si, and M. Yi, “Three-dimensional flat bands and Dirac cones in a pyrochlore superconductor, To appear in *Nat. Phys.*, arXiv:2304.09066 (2023),”.
- [40] R. Yu and Q. Si, *Phys. Rev. B* **86**, 085104 (2012).
- [41] R. Yu and Q. Si, *Phys. Rev. B* **96**, 125110 (2017).
- [42] Y. Komijani and G. Kotliar, *Phys. Rev. B* **96**, 125111 (2017).
- [43] K. Seki and S. Yunoki, *Phys. Rev. B* **96**, 085124 (2017).
- [44] C. Setty, F. Xie, S. Sur, L. Chen, M. G. Vergniory, and Q. Si, arXiv preprint arXiv:2309.14340 (2023).
- [45] A. Blason and M. Fabrizio, *Phys. Rev. B* **108**, 125115 (2023).
- [46] L. Peralta Gavensky, S. Sachdev, and N. Goldman, *Phys. Rev. Lett.* **131**, 236601 (2023).
- [47] J. Zhao, P. Mai, B. Bradlyn, and P. Phillips, *Phys. Rev. Lett.* **131**, 106601 (2023).
- [48] M. Fabrizio, *Nature Communications* **13**, 1 (2022).
- [49] N. Wagner, D. Guerci, A. J. Millis, and G. Sangiovanni, arXiv preprint arXiv:2312.13226 (2023).
- [50] S. Bollmann, C. Setty, U. F. Seifert, and E. J. König, arXiv preprint arXiv:2312.14926 (2023).
- [51] B.-J. Yang, T. Morimoto, and A. Furusaki, *Phys. Rev. B* **92**, 165120 (2015).
- [52] L. de’Medici, A. Georges, and S. Biermann, *Phys. Rev. B* **72**, 205124 (2005).
- [53] R. Yu, J.-X. Zhu, and Q. Si, *Phys. Rev. Lett.* **106**, 186401 (2011).
- [54] E. Zhao and A. Paramakanti, *Phys. Rev. B* **76**, 195101 (2007).
- [55] S. Florens and A. Georges, *Phys. Rev. B* **70**, 035114 (2004).
- [56] W. Ding, R. Yu, Q. Si, and E. Abrahams, *Phys. Rev. B* **100**, 235113 (2019).

SUPPLEMENTARY MATERIAL

Noninteracting Hamiltonian and Dirac nodes

In this section, we present the further details on the kinetic part of the Hamiltonian. As described in the main text, it preserves the $U(1)$ -spin rotational symmetry and, therefore $\mathcal{H}_0^\dagger = [\mathcal{H}_0^\dagger]^\dagger$. In the basis of $\Psi_{\mathbf{k}}^\dagger = [\psi_{Ah}^\dagger, \psi_{Bh}^\dagger, \psi_{Al}^\dagger, \psi_{Bl}^\dagger]$, the Hamiltonian is written as

$$H_0^\dagger(\mathbf{k}) = \begin{pmatrix} t_h \epsilon_{\mathbf{k}} & t_h^{soc} V_{\mathbf{k}} & t_{hl} \epsilon_{\mathbf{k}} & 0 \\ t_h^{soc} V_{\mathbf{k}}^* & -t_h \epsilon_{\mathbf{k}} & 0 & t_{hl} \epsilon_{\mathbf{k}} \\ t_{hl} \epsilon_{\mathbf{k}} & 0 & t_l \epsilon_{\mathbf{k}} & t_l^{soc} V_{\mathbf{k}} \\ 0 & t_{hl} \epsilon_{\mathbf{k}} & t_l^{soc} V_{\mathbf{k}}^* & -t_l \epsilon_{\mathbf{k}} \end{pmatrix}. \quad (9)$$

The parameters $t_{h/l}$, $t_{h/l}^{soc}$ and t_{hl} are chosen to be real, and

$$\epsilon_{\mathbf{k}} = 2(\cos k_x + \cos k_y + \cos k_z), \quad (10)$$

$$V_{\mathbf{k}} = 2(\sin k_x - i \sin k_y) \quad (11)$$

are the form factors related to the nearest neighbor direct hopping and spin-orbit coupling, respectively. Altogether, there are 8 Dirac nodes, with 4 each coming from the heavy (light) orbitals. They are sitting at the momenta $\mathbf{k}_* = (\pi, 0, \pm\pi/2)$ and $\mathbf{k}_* = (0, \pi, \pm\pi/2)$, with the sign of the monopole charge (defined for spin- \uparrow) as shown in Fig. 4. The model we consider has a $U(1)$ spin rotational symmetry (along with time-reversal and inversion symmetries); as a result, the monopole charge of a Dirac point can be defined from a single spin species. Dirac points with other kinds of symmetries can also be considered [51].

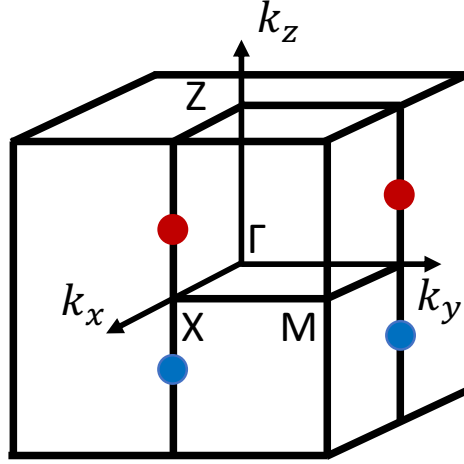


FIG. 4. The position of the Dirac points in the noninteracting limit. The red (blue) indicates a positive (negative) sign of monopole charge (defined for spin- \uparrow component).

Details of the cluster slave spin calculation

In this section, we describe the cluster SS method. As we consider only the interactions on the heavy orbitals, the physical fermionic operators of the heavy orbitals are expressed in terms of the SS and spinon operators as $\psi_{\tau h \sigma}^\dagger = S_{\tau h \sigma}^+ f_{\tau h \sigma}^\dagger$. The intra-orbital Hubbard interaction can be represented by the SS operators as:

$$\mathcal{H}_{int} = \frac{U}{2} \sum_{i, \tau} \left(\sum_{\sigma} S_{\tau h \sigma}^z \right)^2. \quad (12)$$

This representation has a U(1) symmetry. Compared to the Z_2 formulation [52], it has the advantage of allowing the charge degrees of freedom to be expressed in terms of the SS operators alone. Finally, compared to the cluster formulation [53, 54] of the slave rotor approach [55, 56], the small Hilbert space of a slave spin operator facilitates the analysis of the cluster equations.

We then treat the full Hamiltonian at the saddle point level, which contains two decomposed effective Hamiltonian with the SS and spinon operators only. They are specified as follows,

$$\begin{aligned} \mathcal{H}^f = & \sum_{ij,\sigma,\tau\tau'} t_{\tau\tau'}^h e^{i\theta_{ij,h\sigma}^{\tau\tau'}} \langle S_{i\tau h\sigma}^+ S_{j\tau' h\sigma}^- \rangle f_{i\tau h\sigma}^\dagger f_{j\tau' h\sigma} + h.c. + \sum_{ij,\sigma,\tau\tau'} t_{hl} \langle S_{i\tau h\sigma}^+ \rangle f_{i\tau h\sigma}^\dagger \psi_{j\tau' l\sigma} + h.c. \\ & - \lambda \sum_{i\sigma,\tau} f_{i\tau h\sigma}^\dagger f_{i\tau h\sigma} + \mathcal{H}[\psi_{Al}, \psi_{Bl}], \end{aligned} \quad (13)$$

$$\begin{aligned} \mathcal{H}^S = & \sum_{ij,\sigma,\tau\tau'} t_{\tau\tau'}^h \langle e^{i\theta_{ij,h\sigma}^{\tau\tau'}} f_{i\tau h\sigma}^\dagger f_{j\tau' h\sigma} \rangle S_{i\tau h\sigma}^+ S_{j\tau' h\sigma}^- + h.c. + \sum_{ij,\sigma,\tau\tau'} t_{hl} \langle f_{i\tau h\sigma}^\dagger \psi_{j\tau' l\sigma} \rangle S_{i\tau h\sigma}^+ + h.c. \\ & + \lambda \sum_{i\sigma,\tau} \left(S_{i\tau h\sigma}^z + \frac{1}{2} \right) + \mathcal{H}_{int}, \end{aligned} \quad (14)$$

where $\theta_{ij,h\sigma}^{\tau\tau'}$ is the phase factor between the sublattices τ and τ' of the heavy orbitals in unit cells i and j for spin σ , and $t_{AA}^h = -t_{BB}^h = t_h$, $t_{AB}^h = t_{BA}^h = t_h^{soc}$. $\mathcal{H}[\psi_{Al}, \psi_{Bl}]$ is the noninteracting Hamiltonian between the light orbitals. A Lagrangian multiplier λ is introduced to fix the constraint $S_{i\tau h\sigma}^z + 1/2 = f_{i\tau h\sigma}^\dagger f_{i\tau h\sigma}$. Similar to the cluster formulations of other auxiliary-particle approaches [53, 54], we treat the SS Hamiltonian by considering a cluster with two unit cells embedded in an average medium. This leads to a cluster SS Hamiltonian

$$\begin{aligned} \mathcal{H}^S = & \sum_{\tau} t_{\tau\tau}^h \chi_S^{\tau\tau} S_{\tau h\sigma,1}^+ S_{\tau h\sigma,2}^- + h.c. + \sum_{\tau\tau',\tau \neq \tau'} t_{\tau\tau'}^h \chi_S^{\tau\tau'} S_{\tau h\sigma,1}^+ S_{\tau' h\sigma,2}^- + h.c. \\ & + \sum_{\tau} 5t_{\tau\tau}^h \chi_S^{\tau\tau} \langle S_{\tau h\sigma}^+ \rangle \left(S_{\tau h\sigma,1}^- + S_{\tau h\sigma,2}^- \right) + h.c. + \sum_{\tau\tau',\tau \neq \tau'} 3t_{\tau\tau'}^h \chi_S^{\tau\tau'} \langle S_{\tau h\sigma}^+ \rangle \left(S_{\tau' h\sigma,1}^- + S_{\tau' h\sigma,2}^- \right) + h.c. \\ & + \sum_{\sigma,\tau\tau'} 6t_{hl} \chi_S^{f_\tau \psi_{\tau'}} \left(S_{\tau h\sigma,1}^+ + S_{\tau h\sigma,2}^+ \right) + h.c. + \lambda \sum_{\sigma,\tau} \left(S_{\tau h\sigma,1}^z + S_{\tau h\sigma,2}^z + 1 \right) + \mathcal{H}_{int}, \end{aligned} \quad (15)$$

where the subscripts 1, 2 label the two unit cells in the cluster, and

$$\begin{aligned} \chi_S^{\tau\tau} &= \frac{1}{12N_k} \sum_{\mathbf{k}} \epsilon_{\mathbf{k}} \langle f_{\mathbf{k}\tau h\sigma}^\dagger f_{\mathbf{k}\tau h\sigma} \rangle, \\ \chi_S^{\tau\tau'} &= \frac{1}{8N_k} \sum_{\mathbf{k}} V_{\mathbf{k}} \langle f_{\mathbf{k}\tau h\sigma}^\dagger f_{\mathbf{k}\tau' h\sigma} \rangle, \\ \chi_S^{f_\tau \psi_{\tau'}} &= \frac{1}{12N_k} \sum_{\mathbf{k}} \epsilon_{\mathbf{k}} \langle f_{\mathbf{k}\tau h\sigma}^\dagger \psi_{\mathbf{k}\tau' l\sigma} \rangle. \end{aligned} \quad (16)$$

The expectation values appearing in the \mathcal{H}^f are then replaced by the expectation values obtained from \mathcal{H}^S of Eq. (15):

$$\langle S_{i\tau h\sigma}^+ S_{j\tau' h\sigma}^- \rangle = \begin{cases} \langle S_{\tau h\sigma,1}^+ S_{\tau' h\sigma,2}^- \rangle & i, j \in n.n. \\ 0 & otherwise \end{cases} \quad (17)$$

$$\langle S_{i\tau h\sigma}^+ \rangle = \langle S_{\tau h\sigma,1}^+ \rangle = \langle S_{\tau h\sigma,2}^+ \rangle = \sqrt{Z_{\tau h\sigma}}. \quad (18)$$

The spinon Hamiltonian is then written as

$$\begin{aligned} \mathcal{H}^f = & \sum_{ij\sigma,\tau} t_{\tau\tau}^h \chi_f^1 f_{i\tau h\sigma}^\dagger f_{j\tau h\sigma} + h.c. + \sum_{ij\sigma,\tau\tau',\tau \neq \tau'} t_{\tau\tau'}^h \chi_f^2 f_{i\tau h\sigma}^\dagger f_{j\tau h\sigma} + h.c. \\ & + \sum_{ij\sigma,\tau\tau'} t_{hl} \sqrt{Z_{i\tau h\sigma}} f_{i\tau h\sigma}^\dagger \psi_{j\tau' l\sigma} + h.c. - \lambda \sum_{i\sigma,\tau} f_{i\tau h\sigma}^\dagger f_{i\tau h\sigma} + \mathcal{H}[\psi_{Al}, \psi_{Bl}], \end{aligned} \quad (19)$$

with $\chi_f^1 = \langle S_{Ah\sigma,1}^+ S_{Ah\sigma,2}^- \rangle$ and $\chi_f^2 = \langle S_{Ah\sigma,1}^+ S_{Bh\sigma,2}^- \rangle$. Combining the equations from Eq. (15)-(19), it is sufficient to solve the interacting Hamiltonian self-consistently. The variance of χ_f^1 , χ_f^2 and quasiparticle weight is shown in Fig. 5. Both χ_f^1 and χ_f^2 remain to be nonzero throughout, while $Z = 0$ in the OSMP. We note that the filling of each orbital remains 1 throughout the phase diagram.

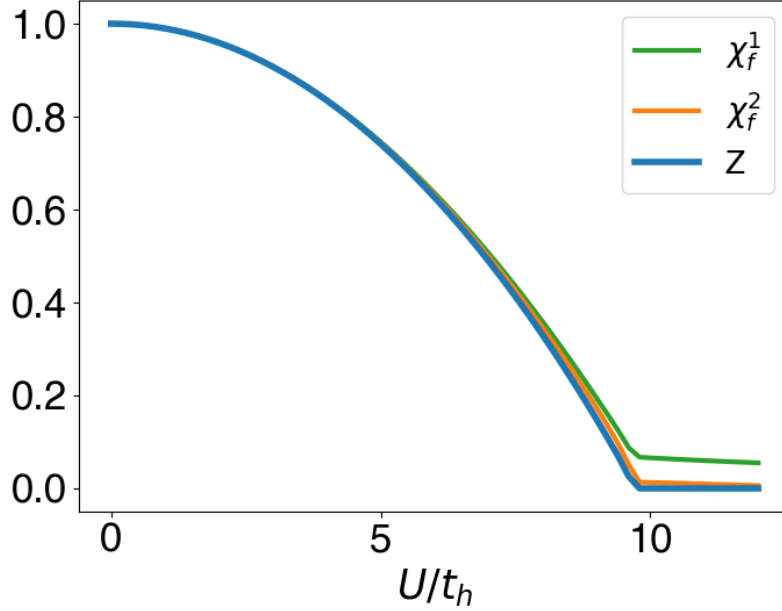


FIG. 5. The quasiparticle weight and the expectation values of the bond operators χ_f^1 and χ_f^2 versus the interaction strength.

Single-particle Green's function in the cluster slave spin method

The cluster SS method gives rise to a translationally-invariant single-particle Green's function of physical electrons. It is obtained by

$$\begin{aligned} G_{\psi}^{\tau\tau'}(\mathbf{k}, \omega) &= \sum_{\mathbf{R}} e^{-i\mathbf{k}\mathbf{R}} G_{\psi}^{\tau\tau'}(\mathbf{R}, \omega) \\ &= G_{\psi}^{\tau\tau'}(\mathbf{0}, \omega) + \sum_{\mathbf{R} \neq \mathbf{0}} e^{-i\mathbf{k}\mathbf{R}} G_{\psi}^{\tau\tau'}(\mathbf{R}, \omega), \end{aligned} \quad (20)$$

where the spin and orbital indices are abbreviated. At zero temperature, the first term is calculated by

$$G_{\psi}^{\tau\tau'}(\mathbf{0}, \omega) = \sum_{\mathbf{k}} \sum_{\alpha} \sum_m \Lambda_{\tau\tau'}^{\alpha, \mathbf{k}} \left[\frac{\langle 0 | S_{\tau,1}^+ | m \rangle \langle m | S_{\tau',1}^- | 0 \rangle (1 - \Theta(\epsilon_{\mathbf{k}}^{\alpha}))}{\omega - E_m - \epsilon_{\mathbf{k}}^{\alpha}} + \frac{\langle 0 | S_{\tau',1}^- | m \rangle \langle m | S_{\tau,1}^+ | 0 \rangle \Theta(\epsilon_{\mathbf{k}}^{\alpha})}{\omega + E_m - \epsilon_{\mathbf{k}}^{\alpha}} \right], \quad (21)$$

where $\Lambda_{\tau\tau'}^{\alpha, \mathbf{k}} = \langle \alpha_{\mathbf{k}} | f_{\mathbf{k}\tau}^\dagger f_{\mathbf{k}\tau'} | \alpha_{\mathbf{k}} \rangle$, with $\epsilon_{\mathbf{k}}^{\alpha}$ ($|\alpha_{\mathbf{k}}\rangle$) the α -th eigenvalues (eigenvectors) of the spinon Hamiltonian. Here, $|m\rangle$ enumerates the eigenvectors of the cluster SS Hamiltonian (Eq. (15)) and E_m denotes the corresponding eigen-energy.

The second term can be obtained from:

$$G_{\psi}^{\tau\tau'}(\mathbf{R}, \omega) = \sum_{\mathbf{k}} \sum_{\alpha} \sum_m e^{i\mathbf{k}\mathbf{R}} \Lambda_{\tau\tau'}^{\alpha, \mathbf{k}} \left[\frac{\langle 0|S_{\tau,1}^+|m\rangle \langle m|S_{\tau',2}^-|0\rangle (1 - \Theta(\epsilon_{\mathbf{k}}^{\alpha}))}{\omega - E_m - \epsilon_{\mathbf{k}}^{\alpha}} + \frac{\langle 0|S_{\tau',2}^-|m\rangle \langle m|S_{\tau,1}^+|0\rangle \Theta(\epsilon_{\mathbf{k}}^{\alpha})}{\omega + E_m - \epsilon_{\mathbf{k}}^{\alpha}} \right], \quad (22)$$

where the operator $S_{\tau,1}^{\pm}$ and $S_{\tau',2}^{\pm}$ are sitting on different unit cells in the SS cluster. The translational invariance of the Green's function is satisfied because all the sites and bonds pick up the SS contributions according to Eqs. (17) and (18).

These two terms can be further separated into coherent and incoherent parts. The coherent part, associated directly with the quasiparticles weights as described by the first term in Eq. (3), is obtained from Eq. (20)-(22) with $m = 0$. The incoherent part, on the other hand, is obtained from Eq. (20)-(22) by summing up terms with $m \neq 0$.